J|A|C|S
ARTICLES
Published on Web 09/17/2005

Probing Ruthenium−Acetylide Bonding Interactions: Synthesis, Electrochemistry, and Spectroscopic Studies of Acetylide−Ruthenium Complexes Supported by Tetradentate Macrocyclic Amine and Diphosphine Ligands

Chun-Yuen Wong,[†] Chi-Ming Che,*[,†] Michael C. W. Chan,[‡] Jie Han,[†] King-Hung Leung,[†,||] David Lee Phillips,[†,||] Kwok-Yin Wong,[§] and Nianyong Zhu[†]

Contribution from the Department of Chemistry and HKU-CAS Joint Laboratory on New Materials, The University of Hong Kong, Pokfulam Road, Hong Kong, China, Department of Biology and Chemistry, City University of Hong Kong, Tat Chee Avenue, Hong Kong, China, and Department of Applied Biology and Chemical Technology, The Hong Kong Polytechnic University, Hunghom, Hong Kong, China

Received May 11, 2005; E-mail: cmche@hku.hk

Abstract: The synthesis and spectroscopic properties of *trans*-[$RuL_4(C{\equiv}CAr)_2$] (L_4 = two 1,2-bis(dimethylphosphino)ethane, $(dmpe)_2$; 1,5,9,13-tetramethyl-1,5,9,13-tetraazacyclohexadecane, 16-TMC; 1,12-dimethyl-3,4:9,10-dibenzo-1,12-diaza-5,8-dioxacyclopentadecane, N_2O_2) are described. Investigations into the effects of varying the [RuL_4] core, acetylide ligands, and acetylide chain length for the [$^-C{\equiv}C(C_6H_4C{\equiv}C)_{n-1}Ph$] and [$^-C{\equiv}C(C_6H_4)_{n-1}Ph$] ($n = 1-3$) series upon the electronic and electrochemical characteristics of *trans*-$[RuL_4(C{\equiv}CAr)_2]^{0/+}$ are presented. DFT and TD-DFT calculations have been performed on *trans*-$[Ru(L')_4(C{\equiv}CAr)_2]^{0/+}$ ($L' = PH_3$ and NH_3) to examine the metal−acetylide π-interaction and the nature of the associated electronic transition(s). It was observed that (1) the relationship between the transition energy and $1/n$ for *trans*-$[Ru(dmpe)_2\{C{\equiv}C(C_6H_4C{\equiv}C)_{n-1}Ph\}_2]$ ($n = 1-3$) is linear, and (2) the sum of the $d_\pi(Ru^{II}) \rightarrow \pi^*(C{\equiv}CAr)$ MLCT energy for *trans*-[Ru(16-TMC or N_2O_2)$(C{\equiv}CAr)_2$] and the $\pi(C{\equiv}CAr) \rightarrow d_\pi(Ru^{III})$ LMCT energy for *trans*-[Ru(16-TMC or N_2O_2)$(C{\equiv}CAr)_2]^+$ corresponds to the intraligand $\pi\pi^*$ absorption energy for *trans*-[Ru(16-TMC or N_2O_2)$(C{\equiv}CAr)_2$]. The crystal structure of *trans*-$[Ru(dmpe)_2\{C{\equiv}C(C_6H_4C{\equiv}C)_2Ph\}_2]$ shows that the two edges of the molecule are separated by 41.7 Å. The electrochemical and spectroscopic properties of these complexes can be systematically tuned by modifying L_4 and Ar to give $E_{1/2}$ values for oxidation of *trans*-$[RuL_4(C{\equiv}CAr)_2]$ that span over 870 mV and λ_{max} values of *trans*-$[RuL_4(C{\equiv}CAr)_2]$ that range from 19 230 to 31 750 cm^{-1}. The overall experimental findings suggest that the π-back-bonding interaction in *trans*-$[RuL_4(C{\equiv}CAr)_2]$ is weak and the [RuL_4] moiety in these molecules may be considered to be playing a "dopant" role in a linear rigid π-conjugated rod.

Introduction

Carbon-rich π-conjugated organic materials such as arylacetylenes[1] and poly(arylene-ethynylene)s[2] possess intriguing nonlinear optical properties and can potentially be employed as polymeric conductors and liquid crystals. These functionalities can be attributed to the π-bonding interaction between the organic moieties, which allows charge delocalization and hence electronic communication along the linear π-conjugated molecular structure. One possible strategy for altering and manipulating the electronic properties of these materials is by incorporating transition metal ion(s) into the π system of the carbon chain, because the electrochemical and spectroscopic characteristics would be an intricate function of the interplay between the metal ion, auxiliary ligands, and π-conjugated groups.[3] If the d_π(metal) and p_π(π-conjugated carbon chain) π-interaction is not strong, the d_π(M) level can be localized and isolated from the π-system of the carbon chain. Under such circumstances, it may be reasonable to view the d_π(M) orbital as a "doped" level in the π-conjugated system, and this would allow the possibility of modifying the properties of the complex

[†] The University of Hong Kong.
[‡] City University of Hong Kong.
[§] The Hong Kong Polytechnic University; address queries on spectroelectrochemical studies to this author.
[||] Address queries on resonance Raman spectroscopy to these authors.

(1) (a) Martin, R. E.; Diederich, F. *Angew. Chem., Int. Ed.* **1999**, *38*, 1350−1377. (b) Stang, P. J.; Diederich, F. *Modern Acetylene Chemistry*; VCH: Weinheim, Germany, 1995. (c) Carter, G. M.; Chen, Y. J.; Rubner, M. F.; Sandman, D. J.; Thakur, M. K.; Tripathy, S. K. In *Non-Linear Optical Properties of Organic Molecules and Crystals*; Chemla, D. S., Zyss, J., Eds.; Academic: Orlando, FL, 1987; Vol. 2, Chapter III-3, p 85.

(2) Reviews: (a) McQuade, D. T.; Pullen, A. E.; Swager, T. M. *Chem. Rev.* **2000**, *100*, 2537−2574. (b) Bunz, U. H. F. *Chem. Rev.* **2000**, *100*, 1605−1644. (c) Tour, J. M. *Acc. Chem. Res.* **2000**, *33*, 791−804. Recent examples: (d) Wilson, J. N.; Bunz, U. H. F. *J. Am. Chem. Soc.* **2005**, *127*, 4124−4125. (e) Wosnick, J. H.; Mello, C. M.; Swager, T. M. *J. Am. Soc. Chem.* **2005**, *127*, 3400−3405. (f) Kwan, P. H.; MacLachlan, M. J.; Swager, T. M. *J. Am. Soc. Chem.* **2004**, *126*, 8638−8639. (g) Tan, C.; Pinto, M. R.; Kose, M. E.; Ghiviriga, I.; Schanze, K. S. *Adv. Mater.* **2004**, *16*, 1208−1212. (h) Beeby, A.; Findlay, K.; Low, P. J.; Marder, T. B. *J. Am. Chem. Soc.* **2002**, *124*, 8280−8284. (i) Cornil, J.; Karzazi, Y.; Brédas, J. L. *J. Am. Chem. Soc.* **2002**, *124*, 3516−3517.

(3) Manna, J.; John, K. D.; Hopkins, M. D. *Adv. Organomet. Chem.* **1995**, *38*, 79−154.

by simply controlling the d_π(M) energy level. In the literature, there have been extensive synthetic studies, structural determinations, and theoretical calculations on transition metal acetylide complexes,[3−5] and materials applications have also been developed in a number of instances.[6−9]

Understanding how metal ions perturb the properties of poly(arylene-ethynylene)s at the molecular level is important for future optoelectronic applications. Hopkins and co-workers have demonstrated that investigations into the nature of metal−acetylide π-interactions through electronic spectroscopy can yield insightful results.[10] In this regard, it would be beneficial to probe the electronic transitions associated with MC≡CR moieties and consequently examine the nature and extent of charge transfer (metal-to-ligand or ligand-to-metal) to provide information on the metal−acetylide bonding interaction(s) in both the ground and the excited states. However, the omnipresence of unsaturated organic auxiliary ligands in most reported MC≡CR complexes has hindered spectral assignment and interpretation of spectroscopic data.

Literature reports on the spectroscopic properties of σ-acetylide metal complexes bearing oligomeric arylacetylide ligands of different chain lengths have appeared.[11−14] Rogers et al. have described the photophysical properties of *trans*-$[Pt(PBu_3)_2\{C{\equiv}C(C_6H_4C{\equiv}C)_{n-1}Ph\}_2]$ ($n = 1-3$),[11] and the nonlinear optical behavior of *trans*-$[ClM(dppe)_2\{C{\equiv}C(C_6H_4C{\equiv}C)_{n-1}Ph\}_2]$ (M = Ru and Os, $n = 1$ and 2, dppe = 1,2-bis(diphenylphosphino)ethane) was reported by the Humphrey group.[5g,12] Che and coworkers have investigated the excited-state properties of $Cy_3PAuC{\equiv}C(C_6H_4C{\equiv}C)_{n-1}Ph$, $Cy_3PAuC{\equiv}C(C_6H_4C{\equiv}C)_nAuPCy_3$[13] ($n = 1-4$), and $[(tpy)(bpy)RuC{\equiv}C(C_6H_4C{\equiv}C)_{n-1}Ph]^+$ ($n = 1-3$, tpy = 2,2′:6′,2″-terpyridine, bpy = 2,2′-bipyridine).[14] We envision that [RuC≡CR] complexes supported by optically transparent auxiliary ligands (L_m) would be an interesting class of compounds for examining metal-to-acetylide and acetylide-to-metal charge-transfer transitions. In a recent related study, we have scrutinized the metal−cumulene bonding interaction in *trans*-$[Cl(16\text{-}TMC)Ru{=}C{=}CHR]^+$, *trans*-$[Cl(16\text{-}TMC \text{ or } (dppm)_2)Ru{=}C{=}C{=}CAr_2]^+$, and *trans*-$[Cl(dppm)_2Os{=}C{=}C{=}CAr_2]^+$ (dppm = bis(diphenylphosphino)methane) using various spectroscopic methods.[15]

As an extension of our investigations to elucidate the nature of ruthenium−carbon multiple bonding interactions, we now present three series of *trans*-$[Ru(C{\equiv}CAr)_2]$ complexes supported by the optically transparent ($\lambda > 300$ nm) 16-TMC, N_2O_2, and dmpe ligands. The effects of changing (1) the $[RuL_4]$ core, (2) acetylide ligands, and (3) acetylide chain length for the $[^-C{\equiv}C(C_6H_4C{\equiv}C)_{n-1}Ph]$ and $[^-C{\equiv}C(C_6H_4)_{n-1}Ph]$ series ($n = 1-3$), upon the electronic properties of *trans*-$[RuL_4(C{\equiv}CAr)_2]$, have been examined. The phosphine-ligated iron and platinum congeners have also been prepared for spectroscopic and electrochemical comparisons. Based on our results and observations, it is appropriate to regard the function of the $[RuL_4]$ unit in these molecules as a "dopant" for the linear π-conjugated system.

Experimental Section

For details on general procedures, supplementary characterization data, and the methods and instrumentations for electrochemistry, spectroelectrochemistry, theoretical calculations, resonance Raman spectroscopy, and X-ray crystallography, please see the Supporting Information.

Synthesis. *trans*-$[M(dmpe)_2(C{\equiv}CAr)_2]$, M = Ru, Ar = Ph (1), $C_6H_4C{\equiv}CPh$ (2), $C_6H_4C{\equiv}CC_6H_4C{\equiv}CPh$ (3), C_6H_4Ph (4), $C_6H_4NMe_2$-4 (5), $C_6H_4C{\equiv}CC_6H_4NMe_2$-4 (6), 2-thienyl (9), C_6H_4−(1,3,4-oxadiazole)−Ph (10); M = Fe, Ar = Ph (20). A mixture of *trans*-$[M(dmpe)_2Cl_2]$ (0.2 mmol), $HC{\equiv}CAr/(CH_3)_3SiC{\equiv}CAr$ (1.0 mmol) and sodium metal (0.10 g, 4.35 mmol) in methanol (30 mL) in the presence of zinc amalgam was refluxed for 12 h. The resultant solid was

(4) (a) Bruce, M. I.; Low, P. J. *Adv. Organomet. Chem.* **2004**, *50*, 179−444. (b) Long, N. J.; Williams, C. K. *Angew. Chem., Int. Ed.* **2003**, *42*, 2586−2617. (c) Szafert, S.; Gladysz, J. A. *Chem. Rev.* **2003**, *103*, 4175−4205. (d) Low, P. J.; Bruce, M. I. *Adv. Organomet. Chem.* **2001**, *48*, 71−286. (e) Lang, H.; George, D. S. A.; Rheinwald, G. *Coord. Chem. Rev.* **2000**, *206−207*, 101−197. (f) Kingsborough, R. P.; Swager, T. M. *Prog. Inorg. Chem.* **1999**, *48*, 123−231. (g) Bruce, M. I. *Coord. Chem. Rev.* **1997**, *166*, 91−119. (h) Nast, R. *Coord. Chem. Rev.* **1982**, *47*, 89−124.

(5) (a) Chui, S. S. Y.; Ng, M. F. Y.; Che, C.-M. *Chem.-Eur. J.* **2005**, *11*, 1739−1749. (b) Yip, S.-K.; Cheng, E. C.-C.; Yuan, L.-H.; Zhu, N.; Yam, V. W.-W. *Angew. Chem., Int. Ed.* **2004**, *43*, 4954−4957. (c) Haskins-Glusac, K.; Pinto, M. R.; Tan, C.; Schanze, K. S. *J. Am. Chem. Soc.* **2004**, *126*, 14964−14971. (d) Antonova, A. B.; et al. *Chem. Commun.* **2004**, 960−961. (e) Costuas, K.; Paul, F.; Toupet, L.; Halet, J.-F.; Lapinte, C. *Organometallics* **2004**, *23*, 2053−2068. (f) Lu, W.; Zhu, N.; Che, C.-M. *J. Am. Chem. Soc.* **2003**, *125*, 16081−16088. (g) Powell, C. E.; Cifuentes, M. P.; Morrall, J. P.; Stranger, R.; Humphrey, M. G.; Samoc, M.; Luther-Davies, B.; Heath, G. A. *J. Am. Chem. Soc.* **2003**, *125*, 602−610. (h) Fernández, F. J.; Venkatesan, K.; Blacque, O.; Alfonso, M.; Schmalle, H. W.; Berke, H. *Chem.-Eur. J.* **2003**, *9*, 6192−9206. (i) Liu, Y.; Jiang, S.; Glusac, K.; Powell, D. H.; Anderson, D. F.; Schanze, K. S. *J. Am. Chem. Soc.* **2002**, *124*, 12412−12413. (j) Field, L. D.; Turnbull, A. J.; Turner, P. *J. Am. Chem. Soc.* **2002**, *124*, 3692−3702. (k) Rigaut, S.; Monnier, F.; Mousset, F.; Touchard, D.; Dixneuf, P. H. *Organometallics* **2002**, *21*, 2654−2661.

(6) (a) Lu, W.; Mi, B.-X.; Chan, M. C. W.; Hui, Z.; Che, C.-M.; Zhu, N.; Lee, S. T. *J. Am. Chem. Soc.* **2004**, *126*, 4958−4971. (b) Schull, T. L.; Kushmerick, J. G.; Patterson, C. H.; George, C.; Moore, M. H.; Pollack, S. K.; Shashidhar, R. *J. Am. Chem. Soc.* **2003**, *125*, 3202−3203. (c) Lu, W.; Chan, M. C. W.; Zhu, N.; Che, C.-M.; He, Z.; Wong, K.-Y. *Chem.-Eur. J.* **2003**, *9*, 6155−6166. (d) Wilson, J. S.; Dhoot, A. S.; Seeley, A. J. A. B.; Khan, M. S.; Köhler, A.; Friend, R. H. *Nature* **2001**, *413*, 828−831. (e) Chan, S.-C.; Chan, M. C. W.; Wang, Y.; Che, C.-M.; Cheung, K.-K.; Zhu, N. *Chem.-Eur. J.* **2001**, *7*, 4180−4190. (f) Chawdhury, N.; Köhler, A.; Friend, R. H.; Wong, W.-Y.; Lewis, J.; Younus, M.; Raithby, P. R. *J. Chem. Phys.* **1999**, *110*, 4963−4970. (g) Ma, Y.-G.; Chan, W.-H.; Zhou, X.-M.; Che, C.-M. *New J. Chem.* **1999**, *23*, 263−265. (h) Köhler, A.; Wittmann, H. F.; Friend, R. H.; Khan, M. S.; Lewis, J. *Synth. Met.* **1996**, *77*, 147−150.

(7) (a) Powell, C. E.; Humphrey, M. G. *Coord. Chem. Rev.* **2004**, *248*, 725−756. (b) Nguyen, P.; Gómez-Elipe, P.; Manners, I. *Chem. Rev.* **1999**, *99*, 1515−1548. (c) Whittall, I. R.; McDonagh, A. M.; Humphrey, M. G.; Samoc, M. *Adv. Organomet. Chem.* **1999**, *43*, 349−405. (d) Whittall, I. R.; McDonagh, A. M.; Humphrey, M. G.; Samoc, M. *Adv. Organomet. Chem.* **1998**, *42*, 291−362. (e) Long, N. J. *Angew. Chem., Int. Ed. Engl.* **1995**, *34*, 21−38.

(8) (a) Ceccon, A.; Santi, S.; Orian, L.; Bisello, A. *Coord. Chem. Rev.* **2004**, *248*, 683−724. (b) Hurst, S. K.; Ren, T. *J. Organomet. Chem.* **2003**, *670*, 188−197. (c) Schwab, P. F. H.; Levin, M. D.; Michl, J. *Chem. Rev.* **1999**, *99*, 1863−1934. (d) Ziessel, R.; Hissler, M.; El-ghayoury, A.; Harriman, A. *Coord. Chem. Rev.* **1998**, *178−180*, 1251−1298. (e) Harriman, A.; Ziessel, R. *Coord. Chem. Rev.* **1998**, *171*, 331−339. (f) Paul, F.; Lapinte, C. *Coord. Chem. Rev.* **1998**, *178−180*, 431−509.

(9) (a) Xu, G.-L.; Zou, G.; Ni, Y.-H.; DeRosa, M. C.; Crutchley, R. J.; Ren, T. *J. Am. Chem. Soc.* **2003**, *125*, 10057−10065. (b) Jiao, H.; Costuas, K.; Gladysz, J. A.; Halet, J.-F.; Guillemot, M.; Toupet, L.; Paul, F.; Lapinte, C. *J. Am. Chem. Soc.* **2003**, *125*, 9511−9522. (c) Paul, F.; Meyer, W. E.; Toupet, L.; Jiao, H.; Gladysz, J. A.; Lapinte, C. *J. Am. Chem. Soc.* **2000**, *122*, 9405−9414. (d) Bruce, M. I.; Low, P. J.; Costuas, K.; Halet, J.-F.; Best, S. P.; Heath, G. A. *J. Am. Chem. Soc.* **2000**, *122*, 1949−1962. (e) Dembinski, R.; Bartik, T.; Bartik, B.; Jaeger, M.; Gladysz, J. A. *J. Am. Chem. Soc.* **2000**, *122*, 810−822. (f) Colbert, M. C. B.; et al. *Organometallics* **1998**, *17*, 3034−3043.

(10) (a) John, K. D.; Stoner, T. C.; Hopkins, M. D. *Organometallics* **1997**, *16*, 4948−4950. (b) Stoner, T. C.; Geib, S. J.; Hopkins, M. D. *Angew. Chem., Int. Ed. Engl.* **1993**, *32*, 409−411. (c) Manna, J.; Geib, S. J.; Hopkins, M. D. *J. Am. Chem. Soc.* **1992**, *114*, 9199−9200. (d) Stoner, T. C.; Dallinger, R. F.; Hopkins, M. D. *J. Am. Chem. Soc.* **1990**, *112*, 5651−5653.

(11) (a) Rogers, J. E.; Cooper, T. M.; Fleitz, P. A.; Glass, D. J.; McLean, D. G. *J. Phys. Chem. A* **2002**, *106*, 10108−10115. (b) Cooper, T. M.; McLean, D. G.; Rogers, J. E. *Chem. Phys. Lett.* **2001**, *349*, 31−36.

(12) Morrall, J. P.; Powell, C. E.; Stranger, R.; Cifuentes, M. P.; Humphrey, M. G.; Heath, G. A. *J. Organomet. Chem.* **2003**, *670*, 248−255.

(13) Chao, H.-Y.; Lu, W.; Li, Y.; Chan, M. C. W.; Che, C.-M.; Cheung, K.-K.; Zhu, N. *J. Am. Chem. Soc.* **2002**, *124*, 14696−14706.

(14) Wong, C.-Y.; Chan, M. C. W.; Zhu, N.; Che, C.-M. *Organometallics* **2004**, *23*, 2263−2272.

(15) Wong, C.-Y.; Che, C.-M.; Chan, M. C. W.; Leung, K.-H.; Phillips, D. L.; Zhu, N. *J. Am. Chem. Soc.* **2004**, *126*, 2501−2514.

collected, washed with MeOH and Et_2O, and recrystallized from CH_2Cl_2/Et_2O (yield: 50−70%). Complex **3**: orange solid, yield 0.10 g, 50%. Anal. Calcd for $C_{60}H_{58}P_4Ru$: C, 71.77; H, 5.82. Found: C, 71.62; H, 5.80. ^{1}H NMR (500 MHz, CD_2Cl_2): δ 1.56 (br, s, 24H, CH_3), 1.70 (br, s, 8H, CH_2), 6.97 (d, $^3J_{HH}$ = 8.3 Hz, 4H, aryl H), 7.22 (d, $^3J_{HH}$ = 8.3 Hz, 4H, aryl H), 7.34−7.37 (m, 6H, aryl H), 7.44−7.48 (m, 8H, aryl H), 7.51−7.53 (m, 4H, aryl H). ^{13}C{^{1}H} NMR (126 MHz, CD_2Cl_2): δ 15.6, 30.2 (dmpe); 88.9, 89.1, 90.8, 92.7 (C≡C); 110.4, 116.0 (RuC≡C); 122.5, 123.1, 123.9, 128.5, 128.6, 130.1, 131.2, 131.3, 131.5, 131.6, 131.7, 131.8 (aryl C). ^{31}P{^{1}H} NMR (202 MHz, CD_2Cl_2): δ 41.2 (s). IR (cm^{-1}): $\nu_{C\equiv C}$ = 2041. FAB-MS: *m*/*z* 1003 [M^+]. See Supporting Information for other complexes.

***trans*-[RuL$_4$(C≡CAr)$_2$], L$_4$ = 16-TMC, Ar = Ph (11), C$_6$H$_4$C≡CPh (12), C$_6$H$_4$Ph (13), 2-fluorene (14), C$_6$H$_4$C$_6$H$_4$Ph (15), C$_6$H$_4$NMe$_2$-4 (16), C$_6$H$_4$−(1,3,4-oxadiazole)−Ph (17), C$_6$H$_4$−(1,3,4-oxadiazole)−C$_6$H$_4$F-4 (18); L$_4$ = N$_2$O$_2$, Ar = Ph (19).** The procedure for **1**−**6** was adopted, but *trans*-[Ru(16-TMC)Cl_2]Cl and *trans*-[Ru(N_2O_2)Cl_2]Cl were used instead of *trans*-[Ru(dmpe)$_2Cl_2$]. Complexes containing 16-TMC ligand were recrystallized from toluene, while **19** was recrystallized from C_6H_6/pentane. Complex **17**: deep red solid, yield 0.13 g, 74%. Anal. Calcd for $C_{48}H_{54}N_8O_2Ru$: C, 65.73; H, 6.21; N, 12.78. Found: C, 65.69; H, 6.16; N, 12.68. ^{1}H NMR (400 MHz, C_6D_6): δ 0.75−1.70 (m, 16H, CH_2), 2.06, 2.11, 2.20, 2.30, 2.36, 2.44 (singlets, 12H, NCH_3), 3.43−4.34 (m, 8H, CH_2), 7.03−7.05 (m, 6H, aryl H), 7.77 (d, 4H, $^3J_{HH}$ = 8.4 Hz, aryl H), 7.98−8.00 (m, 4H, aryl H), 8.29 (d, 4H, $^3J_{HH}$ = 8.4 Hz, aryl H). IR (cm^{-1}): $\nu_{C\equiv C}$ = 1988. FAB-MS: *m*/*z* 875 [M^+]. See Supporting Information for other complexes.

Computational Methodology. Density functional theory (DFT) calculations were performed on *trans*-[$(PH_3)_4$Ru{C≡C(C_6H_4C≡C)$_{n-1}$-Ph}$_2$] (**1′**, *n* = 1; **2′**, *n* = 2; **3′**, *n* = 3), *trans*-[$(PH_3)_4$Ru{C≡C(C_6H_4-C≡C)$_{n-1}$C$_6$H$_4$NMe$_2$-4}$_2$] (**5′**, *n* = 1; **6′**, *n* = 2), *trans*-[$(PH_3)_4$Ru(C≡CC_6H_4-NO_2-4)$_2$] (**7′**), *trans*-[$(NH_3)_4$Ru{C≡C(C_6H_4C≡C)$_{n-1}$Ph}$_2$] (**11′**, *n* = 1; **12′**, *n* = 2), *trans*-[$(PH_3)_2$Pt(C≡CPh)$_2$] (**21′**), *trans*-[$(PH_3)_4$Ru(C≡C-Ph)$_2$]$^+$ (**1′**$^+$), and *trans*-[$(NH_3)_4$Ru(C≡CPh)$_2$]$^+$ (**11′**$^+$), which were used as models for the dmpe- and (16-TMC)-ligated complexes studied in this work. Their electronic ground states were optimized (with C_{2v} symmetry imposed) using the density functional PBE1PBE,[16a] which is a hybrid of the Perdew, Burke, and Ernzerhof exchange and correlation functional[16b] and 25% HF exchange. The Stuttgart small core relativistic effective core potentials were employed for Ru and Pt atoms with their accompanying basis sets.[17] For all other atoms, the 6-31G* basis set was employed.[18] Their vertical transition energies were computed in CH_2Cl_2 at their respective gas-phase optimized ground-state geometries using the time-dependent-DFT (TD-DFT) method employing the same density functional and basis sets in the geometry optimizations. The conductor polarizable continuum model (CPCM)[19] was used to account for solvent effects upon the electronic transition. The nature of the Ru−C bonds were examined using natural bond orbital (NBO)[20] and fragment molecular orbital (FMO) calculations, and charge decomposition analysis (CDA).[21] All DFT, TD-DFT, and NBO calculations were performed using the Gaussian 03 program package[22] while FMO and CDA were performed with AOMix and AOMix-CDA programs,[23] respectively.

Results

Synthesis and Characterization. In this work, the bis(diphosphine) complexes were synthesized by adopting the method developed for *trans*-[Ru(16-TMC)(C≡CAr)$_2$] (**11**−**18**) and *trans*-[Ru(N_2O_2)(C≡CPh)$_2$] (**19**): the precursor *trans*-[ML_4-Cl_2]Cl was treated with excess HC≡CAr or $(CH_3)_3$SiC≡CAr in the presence of NaOMe and zinc amalgam in refluxing methanol (Scheme 1).[24] In the absence of NaOMe and/or zinc amalgam, no reaction was observed upon refluxing for extended periods (over 24 h). Attempts to synthesize *trans*-[Ru(16-TMC)-{C≡C(C_6H_4C≡C)$_2$Ph}$_2$] by adopting the method for **11**−**19** afforded a deep purple solid. FAB-MS analysis of the resultant red Et_2O extract indicated a mixture of HC≡C(C_6H_4C≡C)$_2$Ph and *trans*-[ClRu(16-TMC){C≡C(C_6H_4C≡C)$_2$Ph}] (FAB-MS: *m*/*z* = 302 and 721, respectively). Attempts to prepare *trans*-[Ru(dmpe)$_2$C≡C(C_6H_4C≡C)$_{n-1}$C$_6$H$_4$NO$_2$-4}$_2$] (**7**, *n* = 1; **8**, *n* = 2) by reacting [Ru(dmpe)$_2H_2$] with HC≡C(C_6H_4C≡C)$_{n-1}$C$_6$H$_4$-NO_2-4 gave a mixture of the mono-acetylide *trans*-[ClRu-(dmpe)$_2$C≡C(C_6H_4C≡C)$_{n-1}$C$_6$H$_4$NO$_2$-4}] and bis-acetylide (**7** and **8**) complexes in ca. 1:1 ratio. Hence, the absorption spectra of **7** and **8** are discussed for comparison purposes only. Reports on the coordination chemistry of the [$^-$C≡CC_6H_4-(1,3,4-oxadiazole)-C_6H_4X-4] ligand, which appears in **10**, **17**, and **18**, are sparse in the literature, even though 2,5-diaryl-substituted 1,3,4-oxadiazoles are an established class of electron-transport materials for organic light-emitting-diode (OLED) applications.[25]

Crystal Structures. The molecular structures of **3**−**5** have been determined, and the perspective view of **3** is shown in Figure 1. Crystal data and relevant bond lengths and angles are listed in the Supporting Information. To the best of our knowledge, no crystal structure of a metal complex containing [C≡C−(1,4-C_6H_4−C≡C)$_n$Ph] for $n \geq 2$ has been reported. The Ru−C1 [2.059(2)−2.075(3) Å] and C1−C2 distances [1.178-(4)−1.187(5) Å] in **3**−**5** are typical for Ru(II) acetylide complexes [Ru−C$_\alpha$ = 1.91−2.12 Å, C$_\alpha$−C$_\beta$ = 1.13−1.22 Å].[3] In **3**, the angles within the Ru−C≡C−C and C−C≡C−C units (172.0(5)−179.0(6)°) are close to linearity. The three phenyl rings are not coplanar, with torsional angles of 33.9° and 47.6°. The separations between the two extremes of the molecules are 41.7 Å for **3**, 23.6 Å for **4**, and 19.2 Å for **5**. Examination of the crystal lattices for **3**−**5** revealed no intermolecular $\pi-\pi$ interactions between the conjugated carbon chains.

Electrochemistry. The electrochemical data (obtained in CH_2Cl_2 with 0.1 M [Bu_4N]PF_6 as supporting electrolyte and referenced against the $Cp_2Fe^{+/0}$ couple) are listed in Table 1; selected cyclic voltammograms are depicted in Figure 2. Complexes **1**−**4** display a reversible oxidation couple at $E_{1/2}$ = −0.21 to −0.13 V, with an irreversible oxidation wave at E_{pa} = 0.60−0.62 V. Only subtle changes in the $E_{1/2}$ value (for **1**−**3**, ≤80 mV) for the first oxidation couple are detected as the length of the [$^-$C≡C(C_6H_4C≡C)$_{n-1}$Ph] or [$^-$C≡C(C_6H_4)$_{n-1}$Ph] chain increases. Complex **5** shows three reversible couples with $E_{1/2}$ at −0.49, −0.02, and 0.34 V, but the extended analogue complex **6** only shows a reversible couple at −0.22 V; adsorption was

(16) (a) Adamo, C.; Barone, V. *J. Chem. Phys.* **1999**, *110*, 6158−6170. (b) Perdew, J. P.; Burke, K.; Ernzerhof, M. *Phys. Rev. Lett.* **1996**, *77*, 3865−3868.
(17) Andrae, D.; Haeussermann, U.; Dolg, M.; Stoll, H.; Preuss, H. *Theor. Chim. Acta* **1990**, *77*, 123−141.
(18) (a) Hariharan, P. C.; Pople, J. A. *Theor. Chim. Acta* **1973**, *28*, 213−222. (b) Francl, M. M.; Petro, W. J.; Hehre, W. J.; Binkley, J. S.; Gordon, M. S.; Defree, D. J.; Pople, J. A. *J. Chem. Phys.* **1982**, *77*, 3654−3665.
(19) Barone, V.; Cossi, M. *J. Phys. Chem. A* **1998**, *102*, 1995−2001.
(20) Reed, A. E.; Curtiss, L. A.; Weinhold, F. *Chem. Rev.* **1988**, *88*, 899−926.
(21) (a) Frenking, G.; Fröehlich, N. *Chem. Rev.* **2000**, *100*, 717−774. (b) Dapprich, S.; Frenking, G. *J. Phys. Chem.* **1995**, *99*, 9352−9362.
(22) Frisch, M. J.; et al. *Gaussian 03*, revision B.05; Gaussian, Inc.: Wallingford, CT, 2004.
(23) (a) Gorelsky, S. I. *AOMix program*, rev. 5.93; http://www.sg-chem.net/. (b) Gorelsky, S. I.; Lever, A. B. P. *J. Organomet. Chem.* **2001**, *635*, 187−196.
(24) Choi, M.-Y.; Chan, M. C. W.; Zhang, S.; Cheung, K.-K.; Che, C.-M.; Wong, K.-Y. *Organometallics* **1999**, *18*, 2074−2080.
(25) Adachi, C.; Tsutsui, T.; Saito, S. *Appl. Phys. Lett.* **1990**, *56*, 799−801.

Scheme 1

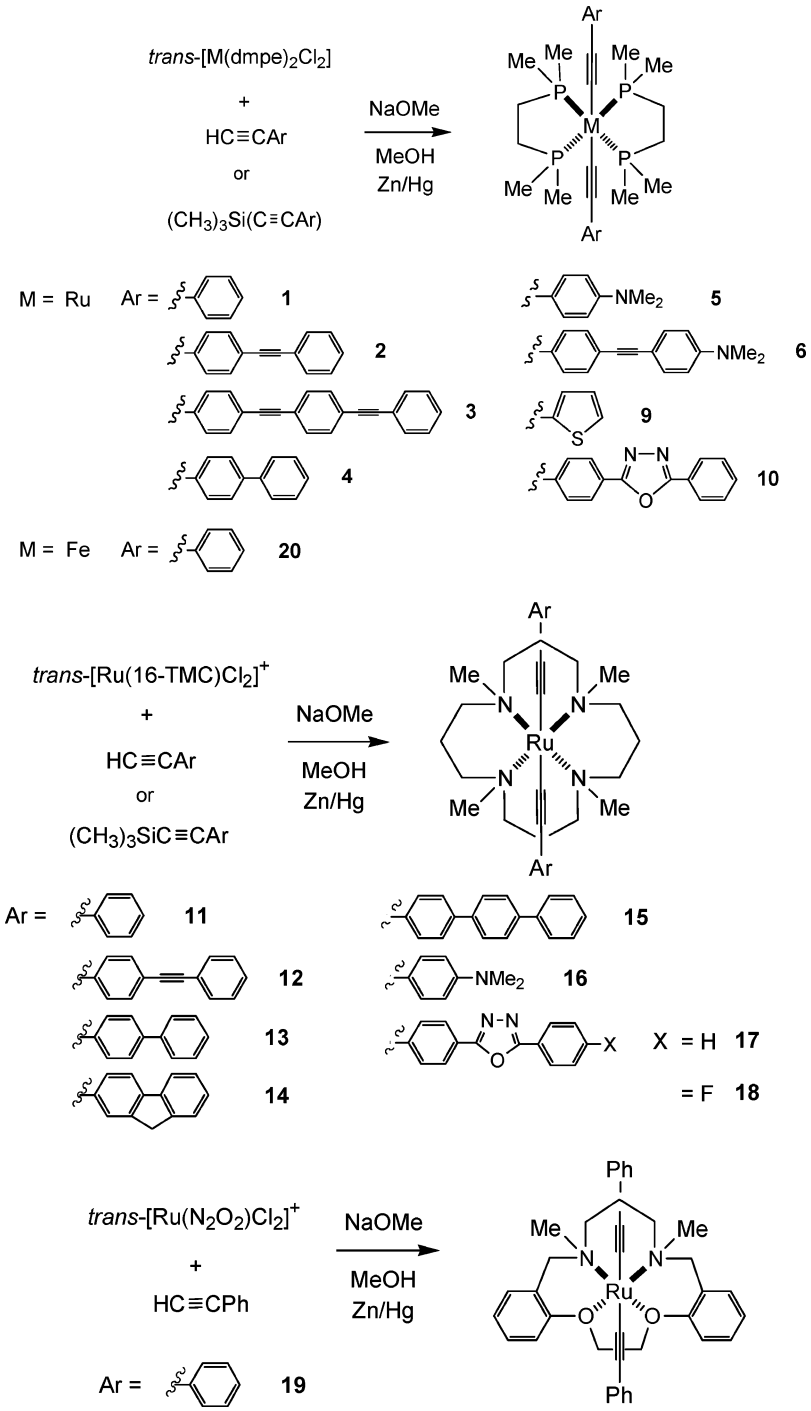

observed at applied potentials above 0.25 V, which hampered further electrochemical studies.

Like the previously reported **11**,[24] **12**−**15** exhibit two quasi-reversible couples at $E_{1/2}$ ca. −0.7 and 0.7 V, while the $E_{1/2}$ values for the (N_2O_2)-ligated complex **19** are slightly shifted to −0.56 and 0.84 V. In contrast, **16** shows three reversible couples with $E_{1/2}$ at −0.95, −0.02, and 0.30 V. With regards to different [ML_m] cores, the dmpe-supported iron derivative **20** displays two reversible couples at $E_{1/2}$ = −0.64 and 0.55 V (Field et al.[26] previously reported $E_{1/2}$ values of −0.61 and 0.54 V vs $Cp_2Fe^{+/0}$), while the platinum complex **21** shows an irreversible oxidation wave at E_{pa} = 0.73 V. For the same [RuL_4] core, the $E_{1/2}$ values for complexes bearing [$^-$C≡CC_6H_4−(1,3,4-oxadiazole)−C_6H_4X-4] are more anodic than those containing [$^-$C≡C(C_6H_4C≡C)$_{n-1}$Ph] or [$^-$C≡C(C_6H_4)$_{n-1}$Ph]. For the *trans*-[ML_4(C≡CPh)$_2$] series, the $E_{1/2}$ values for the *trans*-[ML_4-(C≡CPh)$_2$]$^{+/0}$ couple follow the order: **11** ([Ru(16-TMC)]; −0.77 V) < **20** ([Fe(dmpe)$_2$]; −0.64 V) < **19** ([Ru(N_2O_2)]; −0.56 V) < **1** ([Ru(dmpe)$_2$]; −0.21 V).

Generation of [ML_4(C≡CAr)$_2$]$^+$ by Spectroelectrochemistry. Thin-layer UV−visible spectroelectrochemistry has been employed to acquire the absorption spectra of *trans*-[Ru(dmpe)$_2$-

(26) Field, L. D.; George, A. V.; Laschi, F.; Malouf, E. Y.; Zanello, P. *J. Organomet. Chem.* **1992**, *435*, 347−356.

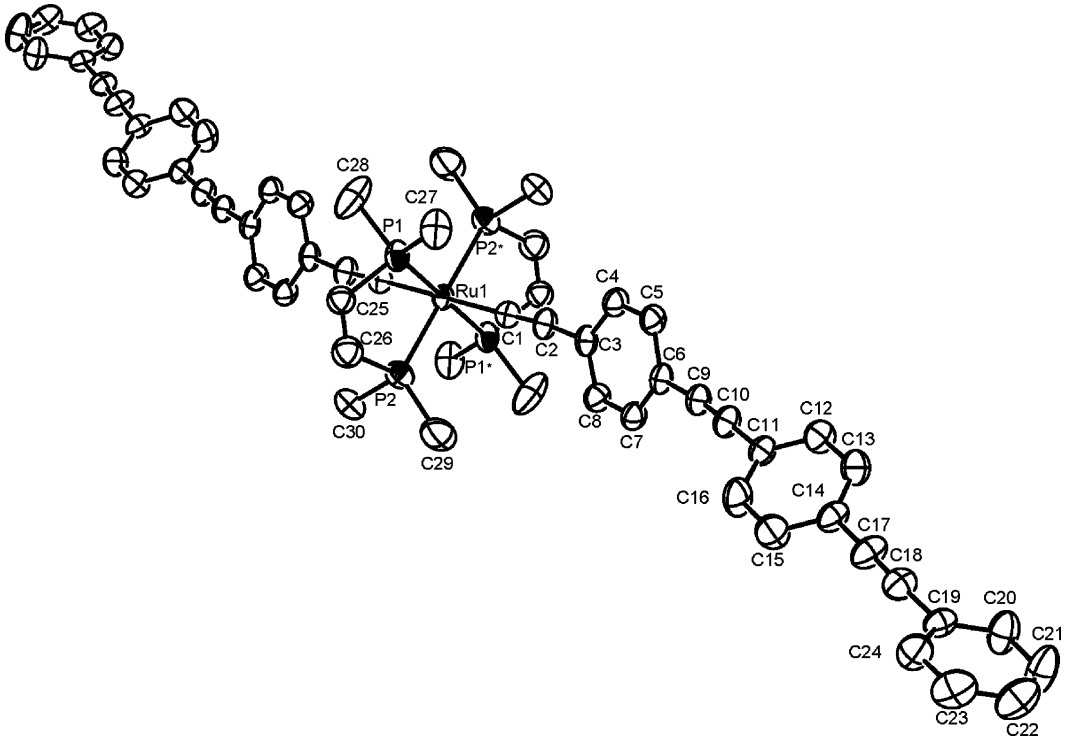

Figure 1. Perspective view of **3** (30% probability ellipsoids).

Table 1. Electrochemical Data for *trans*-[$ML_m(C{\equiv}CAr)_2$], **1**−**6** and **9**−**21**[a]

complex (ML_m, Ar)	$E_{1/2}$/V versus $Cp_2Fe^{+/0}$
1 ($Ru(dmpe)_2$, Ph)	−0.21, 0.62[b]
2 ($Ru(dmpe)_2$, $C_6H_4C{\equiv}CPh$)	−0.14, 0.61[b]
3 ($Ru(dmpe)_2$, $C_6H_4C{\equiv}CC_6H_4C{\equiv}CPh$)	−0.13, 0.61[b]
4 ($Ru(dmpe)_2$, C_6H_4Ph)	−0.21, 0.60[b]
5 ($Ru(dmpe)_2$, $C_6H_4NMe_2$-4)	−0.49, −0.02, 0.34
6 ($Ru(dmpe)_2$, $C_6H_4C{\equiv}CC_6H_4NMe_2$-4)	−0.22[c]
9 ($Ru(dmpe)_2$, 2-thienyl)	−0.22, 0.52[b]
10 ($Ru(dmpe)_2$, C_6H_4−(oxadiazole)−Ph)	−0.08, 0.70[b]
11 (Ru(16-TMC), Ph)	−0.77, 0.72
12 (Ru(16-TMC), $C_6H_4C{\equiv}CPh$)	−0.70, 0.69
13 (Ru(16-TMC), C_6H_4Ph)	−0.73, 0.69
14 (Ru(16-TMC), 2-fluorene)	−0.76, 0.58
15 (Ru(16-TMC), $C_6H_4C_6H_4Ph$)	−0.73, 0.68
16 (Ru(16-TMC), $C_6H_4NMe_2$-4)	−0.95, −0.02, 0.30
17 (Ru(16-TMC), C_6H_4−(oxadiazole)−Ph)	−0.59, 0.89[b]
18 (Ru(16-TMC), C_6H_4−(oxadiazole)−C_6H_4F-4)	−0.60, 0.89[b]
19 ($Ru(N_2O_2)$, Ph)	−0.56, 0.84
20 ($Fe(dmpe)_2$, Ph)	−0.64, 0.55
21 ($Pt(PEt_3)_2$, Ph)	0.73[b]

[a] Supporting electrolyte: 0.1 M [^{n}Bu$_4$N]PF_6 in CH_2Cl_2. $E_{1/2} = (E_{pc} + E_{pa})/2$ at 25 °C for reversible couples. [b] Irreversible; the recorded potential is the anodic peak potential at a scan rate of 100 mV s^{-1}. [c] Adsorption occurs when applied potential is >0.25 V.

$\{C{\equiv}C(C_6H_4C{\equiv}C)_{n-1}Ph\}_2]^+$ (**1**$^+$−**3**$^+$), *trans*-[Ru(16-TMC)($C{\equiv}CAr)_2]^+$ (**11**$^+$−**13**$^+$, **15**$^+$, **17**$^+$, and **18**$^+$), *trans*-[$Ru(N_2O_2)(C{\equiv}CPh)_2]^+$ (**19**$^+$), and *trans*-[$Fe(dmpe)_2(C{\equiv}CPh)_2]^+$ (**20**$^+$); representative isosbestic spectral changes are depicted in Figure 3. For example, the lowest-energy absorption band of **12** at λ_{max} = 485 nm diminishes in intensity and is replaced by a new band at λ_{max} = 786 nm. Similar spectral changes are observed for other complexes [new absorption bands appear at λ_{max} = 711 (for **11**$^+$), 764 (**13**$^+$), 778 (**15**$^+$), 742 (**17**$^+$), 743 (**18**$^+$), 745 (**19**$^+$), 808 nm (**20**$^+$), respectively]. For **1**−**3** (see Supporting Information), no significant increase in absorbance at λ > 800 nm was detected during electrochemical oxidation, while the observation of spectroscopic features in the near-IR region (λ > 1100 nm) was hampered by the limitation of the equipment used in this work. However, absorption at ca. 1100 nm for electrochemically generated *trans*-[$Ru(dppe)_2(C{\equiv}CR)_2]^+$ species was previously reported.[5g]

Absorption Spectroscopy. The UV−vis absorption data of **1**−**21** in CH_2Cl_2 are summarized in Table 2, and representative spectra are depicted in Figure 4. All complexes feature intense absorption bands with $\epsilon_{max} > 10^4$ dm^3 mol^{-1} cm^{-1}. For *trans*-[$ML_m(C{\equiv}CPh)_2$], the transition energy for the lowest dipole-allowed absorption band follows the order: **1** (29 940 cm^{-1}; [ML_m] = [$Ru(dmpe)_2$]) ≈ **21** (29 670 cm^{-1}; [$Pt(PEt_3)_2$]) > **20** (26 810 cm^{-1}; [$Fe(dmpe)_2$]) ≈ **19** (26 670 cm^{-1}; [$Ru(N_2O_2)$]) > **11** (25 190 cm^{-1}; [Ru(16-TMC)]). For complexes with the same [RuL_4] core, the absorption band red-shifts in energy as the conjugation length of the acetylide ligand [$^-C{\equiv}C(C_6H_4C{\equiv}$

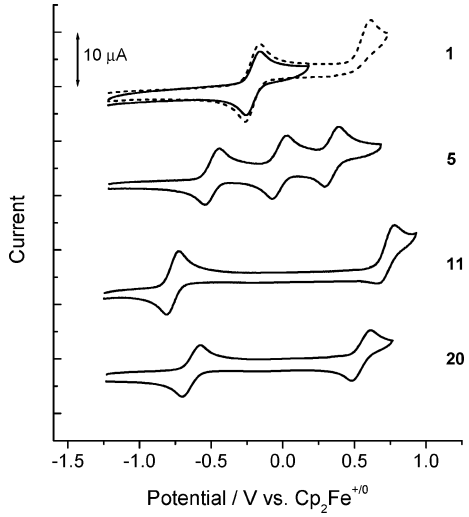

Figure 2. Cyclic voltammograms for selected complexes.

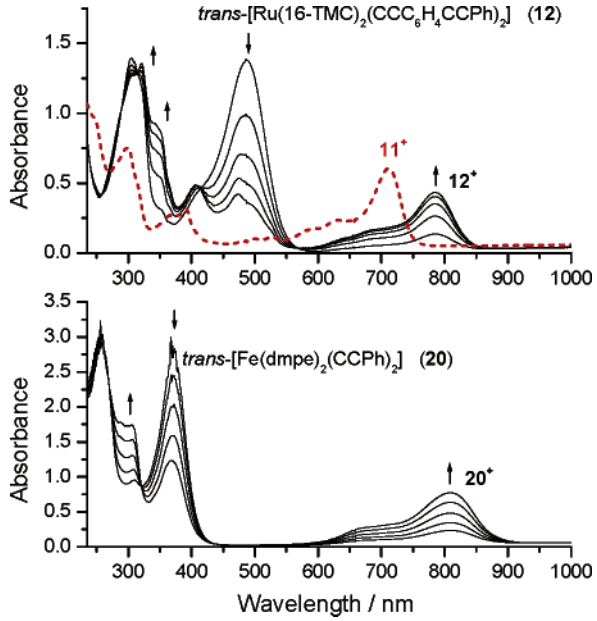

Figure 3. UV−vis absorption spectra of **12** and **20** in CH_2Cl_2 at 298 K during electrochemical oxidation (at −0.3 V vs $Cp_2Fe^{+/0}$, 2-min traces). For comparison, the inserted red line shows the spectrum of *trans*-[Ru(16-TMC)(C≡CPh)$_2$]$^+$ (**11**$^+$) obtained by electrochemical oxidation.

Table 2. UV−Visible Absorption Data for *trans*-[ML_m(C≡CAr)$_2$], **1**−**21**, in CH_2Cl_2 at 298 K

complex (ML_m, Ar)	λ_{max}, nm (ϵ_{max}/dm^3 mol^{-1} cm^{-1})
1 (Ru(dmpe)$_2$, Ph)	288 (sh, 13 600), 334 (40 610)
2 (Ru(dmpe)$_2$, C_6H_4C≡CPh)	292 (21 990), 339 (sh, 16 430), 397 (43 970)
3 (Ru(dmpe)$_2$, C_6H_4C≡CC_6H_4C≡CPh)	323 (54 710), 365 (sh, 21 830), 430 (45 420)
4 (Ru(dmpe)$_2$, C_6H_4Ph)	270 (18 810), 374 (41 080)
5 (Ru(dmpe)$_2$, $C_6H_4NMe_2$-4)	262 (sh, 13 700), 315 (39 660)
6 (Ru(dmpe)$_2$, C_6H_4C≡$CC_6H_4NMe_2$-4)	329 (21 400), 376 (sh, 37 930), 398 (46 380)
7 (Ru(dmpe)$_2$, $C_6H_4NO_2$-4)	287, 331 (sh), 506
8 (Ru(dmpe)$_2$, C_6H_4C≡$CC_6H_4NO_2$-4)	275, 364, 476
9 (Ru(dmpe)$_2$, 2-thienyl)	260 (sh, 12 970), 350 (39 840)
10 (Ru(dmpe)$_2$, C_6H_4−(oxadiazole)−Ph)	265 (sh, 24 000), 301 (38 390), 424 (68 320)
11 (Ru(16-TMC), Ph)	250 (21 970), 328 (sh, 6370), 397 (30 200)
12 (Ru(16-TMC), C_6H_4C≡CPh)	304 (63 850), 485 (69 540)
13 (Ru(16-TMC), C_6H_4Ph)	284 (29 820), 448 (30 170)
14 (Ru(16-TMC), 2-fluorene)	286 (sh, 37 040), 305 (41 910), 458 (47 620)
15 (Ru(16-TMC), $C_6H_4C_6H_4$Ph)	302 (48 970), 464 (27 060)
16 (Ru(16-TMC), $C_6H_4NMe_2$-4)	269 (27 100), 388 (33 000)
17 (Ru(16-TMC), C_6H_4−(oxadiazole)−Ph)	313 (51 140), 518 (56 280)
18 (Ru(16-TMC), C_6H_4−(oxadiazole)−C_6H_4F-4)	313 (52 170), 520 (57 640)
19 (Ru(N_2O_2), Ph)	247 (24 540), 375 (31 300)
20 (Fe(dmpe)$_2$, Ph)	259 (33 910), 373 (38 630)
21 (Pt(PEt_3)$_2$, Ph)	265 (38 300), 289 (32 100), 330 (sh, 43 600), 337 (44 900)

C)$_{n-1}$Ph] or [$^-$C≡C(C_6H_4)$_{n-1}$Ph] is increased. The span in transition energy from n = 1 to 3 for the *trans*-[Ru(16-TMC)-{C≡C(C_6H_4)$_{n-1}$Ph}$_2$] series is only 3640 cm^{-1}, while that for [Ru(16-TMC){C≡C(C_6H_4C≡C)$_{n-1}$Ph}$_2$] from n = 1 to 2 is already 4570 cm^{-1}. The λ_{max} value for **14** (458 nm, Ar = 2-fluorene) is slightly lower in energy than that for **13** (448 nm, Ar = C_6H_4Ph). For *trans*-[Ru(dmpe)$_2${C≡C(C_6H_4C≡C)$_{n-1}C_6H_4NO_2$-4}$_2$], the transition energies for n = 1 (19 760 cm^{-1}; **7**) and 2 (21 010 cm^{-1}; **8**) are similar. For the same [RuL_4] core and value of n, the transition energy for a complex bearing [$^-$C≡C(C_6H_4C≡C)$_{n-1}$Ph] ligand is lower than that containing [$^-$C≡C(C_6H_4)$_{n-1}$Ph]. In addition, λ_{max} values for **17** and **18** (L_4 = 16-TMC, Ar = C_6H_4−(1,3,4-oxadiazole)−C_6H_4X-4) appear at lower energies than **12**−**15** (Ar = C_6H_4C≡CPh, C_6H_4Ph, 2-fluorene, $(C_6H_4)_2$Ph).

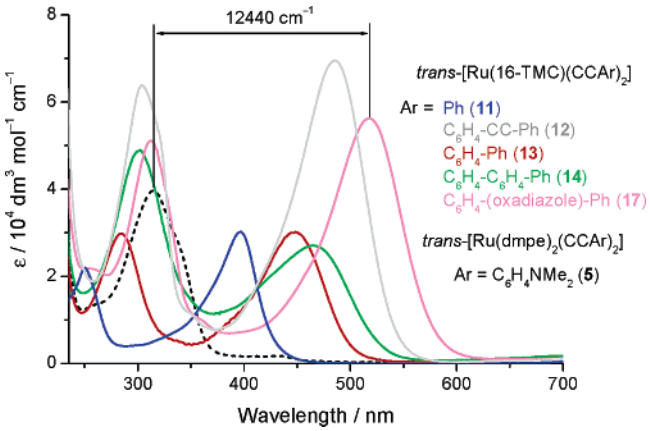

Figure 4. Selected UV−visible absorption spectra of *trans*-[Ru(dmpe)$_2$-(C≡CAr)$_2$] and *trans*-[Ru(16-TMC)(C≡CAr)$_2$] in CH_2Cl_2 at 298 K.

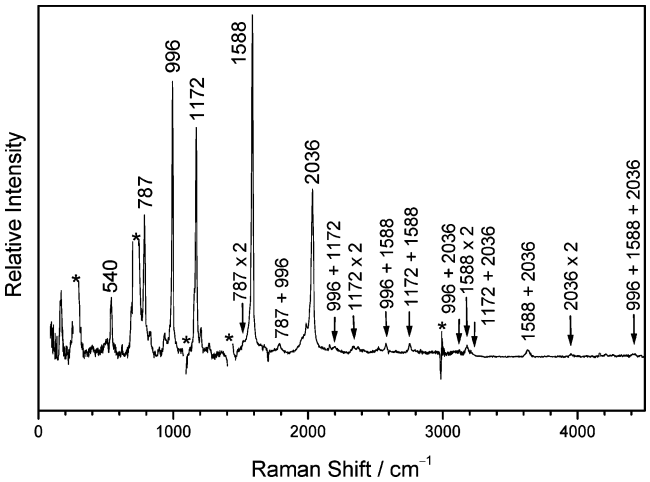

Figure 5. Resonance Raman spectrum of *trans*-[Ru(16-TMC)(C≡CPh)$_2$] (**11**) obtained with 416.0 nm excitation wavelength in CH_2Cl_2 (solvent subtraction marked by *).

Resonance Raman Spectroscopy. Figure 5 shows the resonance Raman spectrum of **11** obtained with 416.0 nm excitation (a similar spectrum was also obtained with 368.9 nm excitation; see Supporting Information). There are 6 fundamental vibrational modes and 13 combination bands and overtones in the spectra. The 2036 and 1588 cm^{-1} Raman bands are assigned as nominal $\nu_{C\equiv C}$ and $\nu_{C=C}$ stretch modes. The resonance Raman intensities and absorption band of **11** (λ_{max} = 397 nm) were simulated to obtain semiquantitative information about the structural changes in the excited state relative to the ground state.[27] We note that the simulations of the resonance Raman and absorption spectra assume that the excited-state frequencies are unchanged from those of the ground state and that this approximation may affect the calculated reorganization energies. Through the simulation (see Supporting Information), it was found that the nominal $\nu_{C\equiv C}$ and $\nu_{C=C}$ stretch modes account for approximately 14% and 45% of the total vibrational reorganization energy, respectively. Moreover, the reorganiza-

(27) Methodology: (a) Leung, K. H.; Phillips, D. L.; Mao, Z.; Che, C.-M.; Miskowski, V. M.; Chan, C.-K. *Inorg. Chem.* **2002**, *41*, 2054−2059. (b) Leung, K. H.; Phillips, D. L.; Tse, M.-C.; Che, C.-M.; Miskowski, V. M. *J. Am. Chem. Soc.* **1999**, *121*, 4799−4803.

Table 3. Comparison of the Vertical Transition Energies for the Model Complexes **1′**−**3′**, **7′**, **11′**, **12′**, **21′**, **1′**$^{+}$, and **11′**$^{+}$ with Their Corresponding Experimental Data

TD-DFT calculations			experimental data	
	excitation energy/cm^{-1} (oscillator strength)	transition		λ_{max}/cm^{-1} (ϵ_{max})
1′	32 810 (1.1499)	MO97 (37% Ru, 61% C_2R) → MO99 (13% Ru, 60% C_2R)	**1**	29 940 (40 610)
2′	25 640 (2.8866)	MO149 (30% Ru, 69% C_2R) → MO150 (5% Ru, 87% C_2R)[a]	**2**	25 190 (43 970)
	31 750 (0.9137)	MO147 (7% Ru, 79% C_2R) → MO151 (3% Ru, 97% C_2R)[a]		34 250 (21 990)
3′	22 780 (3.9780)	MO201 (28% Ru, 71% C_2R) → MO202 (2% Ru, 94% C_2R)[a]	**3**	23 260 (45 430)
	27 620 (1.4858)	MO200 (5% Ru, 84% C_2R) → MO203 (1% Ru, 99% C_2R)[a]		30 960 (54 710)
7′	22 710 (1.2730)	MO119 (39% Ru, 59% C_2R) → MO120 (3% Ru, 92% C_2R)	**7**	19 760
11′	24 510 (0.8753)	MO81 (65% Ru, 33% C_2R) → MO83 (16% Ru, 74% C_2R)	**11**	25 190 (30 200)
	41 490 (0.6776)	MO78 (2% Ru, 91% C_2R) → MO84 (8% Ru, 92% C_2R)[a]		40 000 (21 970)
12′	18 620 (2.0724)	MO133 (60% Ru, 38% C_2R) → MO134 (1% Ru, 96% C_2R)	**12**	20 620 (69 540)
	31 150 (1.3798)	MO130 (1% Ru, 95% C_2R) → MO135 (4% Ru, 95% C_2R)[a]		32 890 (63 850)
21′	28 570 (0.9967)	MO80 (25% Pt, 75% C_2R) → MO81 (20% Pt, 39% C_2R)	**21**	29 670 (44 900)
1′$^{+}$	8550 (0.5310)	MO96β (8% Ru, 69% C_2R) → MO97β (41% Ru, 56% C_2R)	**1**$^{+}$	*b*
11′$^{+}$	14 910 (0.4673)	MO79β (2% Ru, 91% C_2R) → MO81β (64% Ru, 34% C_2R)[a]	**11**$^{+}$	14 060

[a] This absorption originates from several different transitions, and only the most important contribution is shown. [b] Not measured due to instrumental limitation.

tion of the C≡CPh ligand in the excited state is accompanied by reorganization of the Ru−C and Ru−N fragments (Franck−Condon active modes below 1200 cm^{-1}).

DFT Calculations. Calculations have been performed on the model complexes **1′**−**3′**, **5′**−**7′**, **11′**, **12′**, and **21′**, whereby the 16-TMC and $(dmpe)_2$ ligands were replaced by $(NH_3)_4$ and $(PH_3)_4$, respectively, to increase computational efficiency. A summary of the calculation results is provided here (see Supporting Information for a detailed account). For *trans*-$[(PH_3)_4Ru\{C{\equiv}C(C_6H_4C{\equiv}C)_{n-1}Ph\}_2]$ (**1′**−**3′**), the chief contribution to the HOMOs (MO97, MO149, and MO201 for **1′**−**3′**, respectively) originates from the C≡CAr fragments (% of C≡CAr in HOMO > 60%). For *trans*-$[(NH_3)_4Ru\{C{\equiv}C(C_6H_4C{\equiv}C)_{n-1}Ph\}_2]$ (**11′** and **12′**), the HOMOs are dominated by d_{xz}(Ru) (% of d_{xz} in HOMO > 60%). Natural bond orbital (NBO) analyses show that in *trans*-$[M(L')_m(C{\equiv}CAr)_2]$, the populations of the d_{xz}(M) and d_{yz}(M) orbitals of *trans*-$[M(L')_m(C{\equiv}CAr)_2]$ are smaller than those in the bare $[M(L')_m]^{2+}$ core, while the populations of the p_x and p_y orbitals of C_α(acetylide) are increased as compared to the free [$^-$C≡CAr]. In the charge decomposition analysis (CDA) calculations, the M−C≡CAr bonding interaction can be discussed within the framework of the Dewar−Chatt−Duncanson donor−acceptor model as the residual terms (Δ) are essentially zero. The ratio of the values for [$M^{2+} \rightarrow {}^-C{\equiv}CAr$] back-donation (*b*) and [$^-C{\equiv}CAr \rightarrow M^{2+}$] donation (*d*), *b*/*d*, are 0.048−0.050 for *trans*-$[Ru(L')_4(C{\equiv}CAr)_2]$ ($L'_4 = (NH_3)_4$ and $(PH_3)_4$).

The electronic transition(s) for these model complexes in CH_2Cl_2 solvent at 298 K have been investigated using the TD-DFT method. Comparison of the calculated vertical transition energies for the model complexes and the experimental data for the corresponding complexes are summarized in Table 3. The lowest-energy dipole-allowed electronic transitions of *trans*-$[M(L')_m(C{\equiv}CAr)_2]$ (**1′**−**3′**, **7′**, **11′**, **12′**, and **21′**) are assigned to $^1A_1 \rightarrow {}^1A_1$ transitions, which mainly arise from electronic excitation from the HOMO (b_1) to the first unoccupied b_1 MO. For each of the model complexes **1′**−**3′**, **7′**, **11′**, and **12′**, the metal parentage in the excited b_1 MO is smaller than that in the HOMO. Furthermore, the electronic transitions for the oxidized species **1′**$^{+}$ and **11′**$^{+}$ have also been calculated. The lowest-energy absorption band of **1′**$^{+}$ at $\lambda_{max} = 8550$ cm^{-1} originates from the transition involving β-HOMO (MO96β, 8% Ru, 69% C≡CAr) → β-LUMO (MO97β, 41% Ru, 56% C≡CAr), and that of **11′**$^{+}$ at $\lambda_{max} = 14910$ cm^{-1} is mainly associated with the β-HOMO−1 (MO79β, 2% Ru, 91% C≡CAr) → β-LUMO (MO81β, 64% Ru, 34% C≡CAr) transition.

Discussion

***π*-Interaction in Ru−C≡CAr Moiety.** The metal−acetylide π-interaction (π-bonding and/or -back-bonding) has been a subject of considerable interest for many years, and, traditionally, M−C bond distances and $\nu_{C\equiv C}$ values have been employed as indicators.[3,4h] In this work, the $\nu_{C\equiv C}$ values for **11**−**19** (in the range 1986−2012 cm^{-1}) are lower than those of **1**−**10** (2041−2060 cm^{-1}). As the $[Ru(16\text{-TMC})]^{2+}$ and $[Ru(N_2O_2)]^{2+}$ cores should be more electron-rich than $[Ru(dmpe)_2]^{2+}$, this finding indicates the presence of π-back-bonding in the Ru^{II}−C≡CAr moiety. Calculations on model complexes also support the existence of π-back interaction (although this is observed to be weak, as described in later sections): (1) the natural charge on the valence d_π orbitals of Ru (d_{xz} and d_{yz}) decreases and the charge on the valence p_π orbitals of C_α (p_x and p_y) of the acetylide ligand increases upon Ru−C bond formation; (2) charge decomposition analysis (CDA) calculations suggest that the bonding interaction of the M−C≡CAr moiety can be described by the Dewar−Chatt−Duncanson donor−acceptor model and there exists metal-to-acetylide back-donation (*b*), although the acetylide ligand is overall an electron donor (*b*/*d* ≪ 1 as $^-$C≡CAr is anionic). As compared to other ligands such as $^-$Cl and $^-$C≡N, the *b*/*d* ratios for *trans*-$[Ru(L')_4(C{\equiv}CAr)_2]$ (0.048−0.050, $L'_4 = (NH_3)_4$, $(PH_3)_4$) and *trans*-$[(PH_3)_2Pt(C{\equiv}CPh)_2]$ (0.022) lie between those of *trans*-$[Ru(NH_3)_4Cl_2]$ (0.007) and *trans*-$[Ru(NH_3)_4(C{\equiv}N)_2]$ (0.098). Hence, these calculations imply that the arylacetylide ligand in *trans*-$[Ru(L')_m(C{\equiv}CAr)_2]$ acts as a weaker π-acceptor than cyanide, and the metal-to-acetylide back-donation in *trans*-$[Ru(L')_4(C{\equiv}CAr)_2]$ is more significant than that in *trans*-$[(PH_3)_2Pt(C{\equiv}CPh)_2]$.

Because the Ru(II)−C(acetylide) interaction features both σ-bond and π-back-bonding character, it would be of interest to compare the Ru−C(acetylide) distances in this work with those of other ruthenium−carbon bonded complexes bearing similar auxiliary ligand(s). The Ru−C distances in the ruthenium-vinylidene and -allenylidene complexes *trans*-$[Cl(16\text{-TMC})Ru{=}C{=}CHAr]^+$ and *trans*-$[Cl(16\text{-TMC})Ru{=}C{=}C{=}CAr_2]^+$ are 1.78−1.86 Å,[15] which are significantly shorter than those in *trans*-$[(16\text{-TMC})Ru(C{\equiv}CC_6H_4X\text{-}4)_2]$ (2.073−2.077 Å, X = H,

OMe, Cl).[24] An additional worthwhile comparison is with Ru(II) Fischer-type carbene complexes, of which the Ru−C bonds should also exhibit both σ-bond and π-back-bonding character. For example, the Ru−C distance in [(tpy)(bpy)Ru=C(OMe)-($CH_2C_6H_4OMe$-4)]$^{2+}$ is 1.933(6) Å,[14] which is slightly shorter than those in *trans*-[(16-TMC)Ru(C≡CAr)$_2$]. The Ru−C distances in *trans*-[(16-TMC)Ru(C≡CAr)$_2$] are similar to those in *trans*-[(dmpe)$_2$Ru(C≡CAr)$_2$] (2.059−2.075 Å for **3**−**5**), despite the large difference in the $E_{1/2}$ values for the [Ru(16-TMC)]$^{2+}$ and [Ru(dmpe)$_2$]$^{2+}$ cores ($\Delta E_{1/2}$ for the *trans*-[Ru(dmpe)$_2$Cl$_2$]$^{+/0}$ and *trans*-[Ru(16-TMC)Cl$_2$]$^{+/0}$ couples is 520 mV). Taken together, the structural data suggest that the π-back-bonding in Ru(II)−acetylide complexes described in this work is not prominent (alternatively, the lack of correlation with the electrochemical data may reflect the possibility that M−C distances are not sensitive to the strength of π-back-bonding). In this context, Lichtenberger and co-workers have previously employed photoelectron spectroscopy and MO calculations to establish that the predominant iron−acetylide π-interaction in CpFe(CO)$_2$(C≡CR) is the filled/filled type between occupied acetylide π and metal d_π orbitals and that the π-back-bonding is extremely weak.[28]

Redox Potentials for *trans*-[ML$_m$(C≡CAr)$_2$]$^{+/0}$ Couple. Because the dmpe, N_2O_2, and 16-TMC ligands are not redox active from −2 to +1 V vs $Cp_2Fe^{+/0}$, the first electrochemical oxidation of *trans*-[ML$_m$(C≡CAr)$_2$] is evidently metal-centered and can be affected by L$_m$ and Ar. We noted that the two oxidation couples observed for *trans*-[Ru(16-TMC)(C≡CPh)$_2$] (**11**, $E_{1/2}$ = −0.77, 0.72 V)[24] and *trans*-[Fe(dmpe)$_2$(C≡CPh)$_2$] (**20**, $E_{1/2}$ = −0.64, 0.55 V)[26] were previously assigned to M(III/II) and M(IV/III) couples, while a reversible Ru(III)/(II) couple was recorded for the phosphine-supported complex *trans*-[Ru(dppe)$_2$(C≡CPh)$_2$] ($E_{1/2}$ = 0.56 V vs Ag/AgCl; 0.00 V vs $Cp_2Fe^{+/0}$).[5g]

(A) Effects of X upon *trans*-[ML$_4$X$_2$]$^{+/0}$ Couple. A comparison of the $E_{1/2}$ values of *trans*-[ML$_4$X$_2$]$^{+/0}$ couples reveals that the acetylide complexes exhibit lower $E_{1/2}$ values as compared to those bearing Cl$^-$ ligands. For example, the $E_{1/2}$ values for *trans*-[RuL$_4$(C≡CPh)$_2$]$^{+/0}$ (L$_4$ = (dmpe)$_2$, N_2O_2, 16-TMC) are 130, 220, and 140 mV, respectively, more cathodic than *trans*-[RuL$_4$Cl$_2$]$^{+/0}$.[29] The *trans*-[Ru(16-TMC)(C≡CPh)$_2$]$^{+/0}$ couple is 870 mV more cathodic than *trans*-[Ru(16-TMC)(C≡N)$_2$]$^{+/0}$ ($E_{1/2}$ = 0.10 V). These data indicate that $^-$C≡CPh is a superior σ-donor as compared to Cl$^-$ and is unlikely to act as a good π-acceptor.[14]

(B) Effects of [ML$_m$] upon *trans*-[ML$_m$(C≡CAr)$_2$]$^{+/0}$ Couple. Changing the equatorial auxiliary ligands from P-[(dmpe)$_2$] to N- [16-TMC] donors decreases the $E_{1/2}$ value for *trans*-[RuL$_4$(C≡CPh)$_2$]$^{+/0}$ by 560 mV. Interestingly, a similar difference in $E_{1/2}$ values ($\Delta E_{1/2}$) of 520 mV between the *trans*-[Ru(dmpe)$_2$Cl$_2$]$^{+/0}$ (−0.08 V)[29c] and *trans*-[Ru(16-TMC)Cl$_2$]$^{+/0}$ (−0.60 V)[29a] couples has been reported. The $\Delta E_{1/2}$ for the *trans*-[M(dmpe)$_2$(C≡CPh)$_2$]$^{+/0}$ couples for Ru (**1**) and Fe (**20**) is 430 mV, while a similar $\Delta E_{1/2}$ (460 mV) is apparent for the corresponding *trans*-[M(dmpe)$_2$Cl$_2$]$^{+/0}$ couples. These observations illustrate the possibility of tuning the redox potential of the [ML$_4$(C≡CAr)$_2$]$^{+/0}$ couple over a wide range through variation of the auxiliary ligand and metal center. This contrasts with *trans*-[Cl(16-TMC or (dppm)$_2$)Ru=C=C=CAr$_2$]$^+$, in which the electrochemical reactions are neither metal- nor ligand-centered.[15] In DFT calculations for the model complexes, the HOMO energies increase in the order **21′** (−5.71 eV) < **3′** (−5.11 eV) ≈ **2′** (−5.10 eV) ≈ **1′** (−5.09 eV) ≈ **6′** (−4.85 eV) < **5′** (−4.49 eV) < **12′** (−4.11 eV) ≈ **11′** (−3.93 eV); this parallels the experimental trend of the oxidation potentials for the corresponding complexes.

(C) Effects of Ar upon *trans*-[ML$_m$(C≡CAr)$_2$]$^{+/0}$ Couple. The effects of different conjugation lengths for the acetylide ligands upon the *trans*-[RuL$_4$\{C≡C(C$_6$H$_4$C≡C)$_{n-1}$Ph\}$_2$]$^{+/0}$ and *trans*-[RuL$_4$\{C≡C(C$_6$H$_4$)$_{n-1}$Ph\}$_2$]$^{+/0}$ couples are small, for example, $E_{1/2}$ for **1**$^{+/0}$ (n = 1, $E_{1/2}$ = −0.21 V) ≈ **2**$^{+/0}$ (n = 2, −0.14 V) ≈ **3**$^{+/0}$ (n = 3, −0.13 V), while $E_{1/2}$ for **11**$^{+/0}$ (n = 1, $E_{1/2}$ = −0.77 V) ≈ **12**$^{+/0}$ (n = 2, −0.70 V). As lowering of π^*(C≡CAr) level with higher n has been demonstrated by electronic spectroscopy (see discussion below), one may expect lower $E_{1/2}$ values as n increases due to a stronger π-back-bonding interaction between Ru and C≡CAr. However, the experimental findings show that, for a given [RuL$_4$] core, the $E_{1/2}$[Ru(III/II)] values for different values of n are similar. This suggests that the π-interaction between Ru and C≡CAr is weak and is also consistent with the metal-centered assignment for the *trans*-[RuL$_4$(C≡CAr)$_2$]$^{+/0}$ couple. *We therefore propose to regard the d_π(Ru^{II}) orbital as a "doped" level that exists between the π(C≡CAr) and π^*(C≡CAr) orbitals* (see below). This proposal is also supported by the $\nu_{C\equiv C}$ stretching frequencies, which are insensitive to the lengthening effect of the conjugated acetylide ligands.

(D) Effects of 4-Dimethylamino and Oxadiazole Substituents. The cyclic voltammograms of **5** and **16** feature three reversible oxidation waves ($E_{1/2}$ = −0.49, −0.02, and 0.34 V for **5**; −0.95, −0.02, and 0.30 V for **16**). As **1** and **11** show only one reversible couple in this potential region ($E_{1/2}$ = −0.21 and −0.77 V, respectively), some of the oxidation waves in **5** and **16** apparently involve the NMe$_2$ moiety. The first couple is assigned as being metal-centered in nature ($\Delta E_{1/2}$ for **5** and **16** is 460 mV), and the second and third couples as NMe$_2$-centered oxidations, for which the $E_{1/2}$ values are similar for both complexes. As the two NMe$_2$ groups are not oxidized at the same potential, the existence of electronic communication between the two termini of *trans*-[Ru(16-TMC or (dmpe)$_2$)-(C≡CC$_6$H$_4$NMe$_2$-4)$_2$] (N−N distance = 17.9 Å for **5**, from the crystal structure) is demonstrated. Marder and co-workers have recently described the Pt(II) bis-(triarylamine)acetylide complex *trans*-[Pt(PEt$_3$)$_2$\{C≡C−1,4-C$_6$H$_4$−N(C$_6$H$_4$OMe-4)$_2$\}$_2$],[30] the electrochemistry of which involves two overlapping reversible oxidations due to the triarylamine groups, thus implying electronic coupling through the acetylide−Pt−acetylide bridge. Although one may not expect to detect long-range electronic communication in **5** and **16** as the π-interaction in Ru(II)−acetylide species is weak, the π-interaction will be strengthened upon oxidation to Ru(III) because for this species the delocalized cumulene-like mesomeric form becomes more important.[9]

(28) (a) Lichtenberger, D. L.; Renshaw, S. K.; Bullock, R. M. *J. Am. Chem. Soc.* **1993**, *115*, 3276−3285. (b) Lichtenberger, D. L.; Renshaw, S. K.; Wong, A.; Tagge, C. D. *Organometallics* **1993**, *12*, 3522−3526.
(29) (a) Che, C.-M.; Wong, K.-Y.; Poon, C.-K. *Inorg. Chem.* **1986**, *25*, 1809−1813. (b) Che, C.-M.; Tang, W.-T.; Wong, W.-T.; Lai, T.-F. *J. Am. Chem. Soc.* **1989**, *111*, 9048−9056. (c) Champness, N. R.; Levason, W.; Pletcher, D.; Webster, M. *J. Chem. Soc., Dalton Trans.* **1992**, 3243−3247.
(30) Jones, S. C.; Coropceanu, V.; Barlow, S.; Kinnibrugh, T.; Timofeeva, T.; Brédas, J.-L.; Marder, S. R. *J. Am. Chem. Soc.* **2004**, *126*, 11782−11783.

We note that the $E_{1/2}$ values for the metal-centered oxidation of **5** and **16** are 280 and 180 mV more cathodic than **1** and **11**, respectively. This may be explained by the nature of the electron-donating NMe_2 groups, which stabilize the oxidized species *trans*-$[RuL_4(C{\equiv}CAr)_2]^+$ via the N lone-pairs. Although electrochemical investigation of the more conjugated derivative **6** was hampered by an adsorption process, the fact that the metal-centered oxidation ($E_{1/2} = -0.22$ V) occurs at a potential similar to **1** ($E_{1/2} = -0.21$ V) suggests minimal electronic communication between the two N termini.

(E) Nature of *trans*-$[ML_m(C{\equiv}CAr)_2]^{2+/+}$ Couple. Regarding the second oxidation couple for these complexes, such as *trans*-$[Ru(16\text{-TMC})(C{\equiv}CPh)_2]^{2+/+}$ ($E_{1/2} = 0.72$ V, previously assigned as Ru(IV/III) couple[24]) and *trans*-$[Fe(dmpe)_2(C{\equiv}CPh)_2]^{2+/+}$ ($E_{1/2} = 0.55$ V, previously assigned as Fe(IV/III) couple[26]), the $E_{1/2}$ values are similar and comparable to the E_{pa} of the irreversible oxidation wave of *trans*-$[Ru(dmpe)_2(C{\equiv}CPh)_2]$ at $E_{pa} = 0.62$ V. The nature of these oxidations is unlikely to be metal-centered because a substantial shift in $E_{1/2}$ upon changing from Ru to Fe is expected (note that the $\Delta E_{1/2}$ for M(III/II) couples of **1** and **20** is 430 mV). Moreover, DFT calculations on the model complex *trans*-$[Ru(NH_3)_4(C{\equiv}CPh)_2]^+$ (**11′**$^+$) indicate that the SOMO is [C≡CPh]-dominated (71% C≡CPh, 29% Ru). Thus, we suggest that it is appropriate to reassign the *trans*-$[Ru(16\text{-TMC})(C{\equiv}CPh)_2]^{2+/+}$ couple as a ligand-centered oxidation. In line with this assignment, the E_{pa} for **21** (*trans*-$[Pt(PEt_3)_2(C{\equiv}CPh)_2]^{+/0}$: 0.73 V) occurs at a potential similar to the ligand-centered oxidation of **11** [DFT calculations also show that the energy of the SOMO in **11′**$^+$ (−5.98 eV) is similar to that of the HOMO in **21′** (−5.71 eV)]. Furthermore, the HOMO of the model complex *trans*-$[Pt(PH_3)_2(C{\equiv}CPh)_2]$ (**21′**) is also [C≡CPh]-dominated (75% C≡CPh, 25% Pt), and hence the *trans*-$[Pt(PEt_3)_2(C{\equiv}CPh)_2]^{+/0}$ oxidation is also assigned as ligand-centered in nature.

In this work, *trans*-$[Ru(16\text{-TMC})(C{\equiv}CPh)_2]$ (**11**, $E_{1/2} = -0.77$ V) and *trans*-$[Pt(PEt_3)_2(C{\equiv}CPh)_2]$ (**21**, $E_{pa} = 0.73$ V) can be considered as two extreme cases for probing the metal−acetylide interaction. In **11**, the calculated HOMO (**11′**, 65% Ru) and the $[ML_m(C{\equiv}CAr)_2]^{+/0}$ couple are metal-based, while for **21**, the HOMO is ligand-based (**21′**, 25% Pt), and the E_{pa} of $[ML_m(C{\equiv}CAr)_2]^{+/0}$ arises mainly from acetylide oxidation. For *trans*-$[Ru(dmpe)_2(C{\equiv}CPh)_2]$ (**1**), both the potential for the first oxidation ($E_{1/2} = -0.21$ V) and the ruthenium parentage of the HOMO for **1′** are between those of **11′** and **21′**. Collectively, this indicates a possible correlation between $E_{1/2}$ of *trans*-$[ML_m(C{\equiv}CAr)_2]^{+/0}$ and the degree of metal character in the HOMO of *trans*-$[ML_m(C{\equiv}CAr)_2]$.

Insight from Electronic and Resonance Raman Spectroscopy. Complexes **1**−**21** exhibit intense dipole-allowed absorption bands in the UV−visible region with ϵ_{max} in excess of 10^4 $dm^3\ mol^{-1}\ cm^{-1}$. As the chosen auxiliary ligands (dmpe, 16-TMC, and N_2O_2) are optically transparent in the UV−visible region, the electronic transitions for **1**−**21** are predominantly associated with the *trans*-$[M(C{\equiv}CAr)_2]$ core. We are interested in the low-energy dipole-allowed transition of these complexes and will restrict our discussion to this absorption in the following sections.

(A) Effects of $[ML_m]$ Core. The nature of the transitions depends on the $[ML_m]$ core. Taking the series *trans*-$[ML_m(C{\equiv}CPh)_2]$ as an example, λ_{max} decreases in energy in the order **1** ($[Ru(dmpe)_2]$) > **19** ($[Ru(N_2O_2)]$) ≈ **20** ($[Fe(dmpe)_2]$) > **11** ($[Ru(16\text{-TMC})]$) (λ_{max} = 29 940, 26 670, 26 810, and 25 190 cm^{-1}, respectively); significantly, this parallels the trend for $E_{1/2}$-[M(III/II)]. For *trans*-$[ML_m(C{\equiv}CC_6H_4C{\equiv}CPh)_2]$, changing the $[ML_m]$ core from $[Ru(dmpe)_2]$ (**2**, $E_{1/2} = -0.14$ V) to [Ru(16-TMC)] (**12**, $E_{1/2} = -0.70$ V) results in a decrease in transition energy of 4570 cm^{-1}. The correlation between the $E_{1/2}$[M(III/II)] value and electronic transition energy is consistent with the MLCT assignment. The TD-DFT calculations performed on the model complexes reveal that the lowest-energy electronic transition for **1′** and **11′** are $^1A_1 \rightarrow {}^1A_1$ in nature (excitation of electrons from the HOMOs (b_1) to the first unoccupied b_1 MOs). For **1′**, an electron is excited from a mainly ligand-based HOMO (37% Ru, 61% C≡CPh) to a ligand-dominated MO (13% Ru, 60% C≡CPh), whereas for **11′**, an electron is excited from a metal-based HOMO (65% Ru, 33% C≡CPh) to a ligand-dominated MO (16% Ru, 74% C≡CPh). Thus, although the electronic transition for **1**−**3**, **11**, and **12** may be described as displaying MLCT character, the charge-transfer character associated with **1**−**3** is relatively small as compared to **11** and **12**. Calculations on the Pt model complex **21′** show that an electron is excited from the [C≡CAr]-localized HOMO (25% d_{xz}(Pt), 75% C≡CAr) to the LUMO that is composed of p_x(Pt), PH_3, and C≡CAr (20%, 41%, and 39%, respectively); thus the transition is assigned as intraligand in nature.

(B) Effects of Conjugation Length *n*. The lowest-energy transition red-shifts when the conjugation length *n* of the acetylide ligand [$^-$C≡C($C_6H_4C{\equiv}C)_{n-1}$Ph] or [$^-$C≡C($C_6H_4)_{n-1}$Ph] increases for the same $[RuL_4]$ core. For *trans*-$[Ru(dmpe)_2\{C{\equiv}C(C_6H_4C{\equiv}C)_{n-1}Ph\}_2]$ (**1**−**3**), the transition energies fall in the order: **1** ($n = 1$, 29 940 cm^{-1}) > **2** ($n = 2$, 25 190 cm^{-1}) > **3** ($n = 3$, 23 260 cm^{-1}). In *trans*-$[Ru(16\text{-TMC})\{C{\equiv}C(C_6H_4)_{n-1}Ph\}_2]$ (**11**, **13**, and **15**), the λ_{max} energies red-shift by 3640 cm^{-1} when *n* changes from 1 (**11**, 25 190 cm^{-1}) to 3 (**15**, 21 550 cm^{-1}). These red-shifted transitions are consistent with greater conjugation across the [$^-$C≡C($C_6H_4C{\equiv}C)_{n-1}$Ph] and [$^-$C≡C($C_6H_4)_{n-1}$Ph] chains with increasing *n* values, which result in lower π^* levels. Previously, Che and co-workers have examined the relationship of the $^1(\pi\pi^*)$ absorption or $^3(\pi\pi^*)$ phosphorescent emission energy with the acetylide/arylacetylide chain length *n* in $(Cy_3P)Au(C{\equiv}C)_nAu(PCy_3)$,[31] $(Cy_3P)AuC{\equiv}C(C_6H_4C{\equiv}C)_{n-1}Ph$, and $(Cy_3P)AuC{\equiv}C(C_6H_4C{\equiv}C)_nAu(PCy_3)$,[13] and linear relationships were obtained by plotting the absorption or emission energy versus 1/*n*. In this work, a linear relationship is also derived for the absorption energy and 1/*n* for *trans*-$[Ru(dmpe)_2\{C{\equiv}C(C_6H_4C{\equiv}C)_{n-1}Ph\}_2]$ (**1**−**3**) (Figure 6). Extrapolation of the line to $n = \infty$ affords an estimated value of ∼498 nm (20 080 cm^{-1}) for the absorption energy. In addition, we note that the absorption energy for the calculated model series *trans*-$[Ru(PH_3)_4\{C{\equiv}C(C_6H_4C{\equiv}C)_{n-1}Ph\}_2]$ for $n = \infty$ is estimated to be ∼556 nm (17 990 cm^{-1}). It is particularly interesting to compare the limiting absorption energy (i.e., for $n = \infty$) for related acetylene and metal−acetylide moieties. For alkyl-substituted poly(*p*-phenylene-ethynylene)s (PPEs), the limiting absorption energy is around 388 nm,[32] while those for $(Cy_3P)AuC{\equiv}C(C_6H_4C{\equiv}C)_{n-1}Ph$ and $(Cy_3P)AuC{\equiv}C(C_6H_4C{\equiv}C)_nAu(PCy_3)$ are in the 399−411 nm range,[13] and an energy of ca. 404 nm was derived

(31) Lu, W.; Xiang, H.-F.; Zhu, N.; Che, C.-M. *Organometallics* **2002**, *21*, 2343−2346.
(32) Mangel, T.; Eberhardt, A.; Scherf, U.; Bunz, U. H. F.; Müllen, K. *Macromol. Rapid Commun.* **1995**, *16*, 571−580.

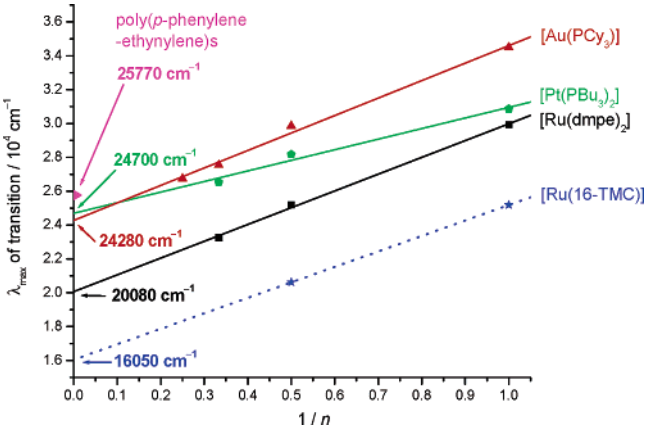

Figure 6. Plot of the lowest transition energy against 1/*n* for *trans*-[ML_m-{C≡C(C_6H_4C≡C)$_{n-1}$Ph}$_2$] [ML_m = Ru(dmpe)$_2$, Pt(PBu_3)$_2$,[11] Ru(16-TMC)], (PCy_3)AuC≡C(C_6H_4C≡C)$_{n-1}$Ph,[13] and alkyl-substituted poly(*p*-phenylene-ethynylene)s.[32]

for *trans*-[Pt(PBu_3)$_2${C≡C(C_6H_4C≡C)$_{n-1}$Ph}$_2$].[11] These energies are significantly higher than that for *trans*-[Ru(dmpe)$_2${C≡C(C_6H_4C≡C)$_{n-1}$Ph}$_2$] (498 nm), thus signifying the involvement of the [Ru(dmpe)$_2$] core in the electronic transition. The data for *trans*-[Ru(16-TMC){C≡C(C_6H_4C≡C)$_{n-1}$Ph}$_2$] (*n* = 1, 2) are also plotted in Figure 6. Assuming that a linear relationship is also valid in this system, the limited value is estimated to be 623 nm.

It has been established that the relationship of the transition energy versus 1/*n* is linear for intraligand transitions of π-conjugated oligomeric organic materials.[33,34] *In this work, a linear relationship has been obtained for trans-[Ru(dmpe)$_2${C≡C(C_6H_4C≡C)$_{n-1}$Ph}$_2$] (**1**−**3**), the transition of which involves some MLCT character*. We have provided evidence to indicate that the π-interaction between Ru(II) and [C≡CAr] in **1**−**3** is weak. For the [Ru(C≡CAr)$_2$] moiety, the $d_\pi(Ru^{II})$ level can therefore be regarded as being localized and isolated from the π-system, so that the $d_\pi(Ru^{II})$ energy level is virtually constant for all *n* and thus 1/*n* values. If the π*(C≡CAr) energy level decreases linearly with 1/*n* as expected, then the MLCT transition energy, that is, $E[\pi^*(C{\equiv}CAr)] - E[d_\pi(Ru^{II})]$, would also vary linearly with 1/*n*, as observed for **1**−**3**.

(C) Effects of Ar. (1) The transition energy for **14** (21 830 cm^{-1}, Ar = 2-fluorene) is slightly lower than that for **13** (22 320 cm^{-1}, Ar = C_6H_4Ph). Because the additional −CH_2− unit of the 2-fluorene group restricts the rotation of the two phenyl rings to afford a more coplanar configuration and hence greater π-conjugation, the lowering of the transition energy is plausible. (2) The transition energies for complexes bearing [$^-$C≡CC_6H_4−(1,3,4-oxadiazole)−C_6H_4X] (**17** and **18**: λ_{max} = 19 310 and 19 230 cm^{-1}, respectively) are lower than that with [$^-$C≡C(C_6H_4)$_2$Ph] (**15**, 21 550 cm^{-1}). This can be rationalized by the presence of the heteroatoms (N and O), which lower the π* energy. (3) For the nitro derivatives *trans*-[Ru(dmpe)$_2${C≡C(C_6H_4C≡C)$_{n-1}$$C_6H_4$$NO_2$-4}$_2$], the transition energy for **7** (*n* = 1, λ_{max} = 19 760 cm^{-1}) is slightly lower than that for **8** (*n* = 2, 21 010 cm^{-1}).[35] TD-DFT calculations suggest that the charge-transfer character associated with **7** is larger than that for **1**−**3** due to the presence of the electron-withdrawing NO_2 groups. The increase in transition energy from **7** to **8** is likely due to a decrease in the influence of the NO_2 groups when the acetylide ligand is lengthened.

(D) Oxidation State of M and Acetylide-to-Ruthenium(III) LMCT Transitions. The absorption spectra of *trans*-[Ru(dmpe)$_2$(C≡CAr)$_2$]$^+$, *trans*-[Ru(16-TMC)(C≡CAr)$_2$]$^+$ and *trans*-[Fe(dmpe)$_2$(C≡CAr)$_2$]$^+$ were recorded in situ by electrochemical oxidation of their corresponding M(II) precursors. Previously, we obtained vibronically structured absorption bands for *trans*-[Ru(16-TMC)(C≡CAr)$_2$]$^+$ with λ_{max} = 716−768 nm, which were assigned as $\pi(C{\equiv}CAr) \rightarrow d_\pi(Ru^{III})$ LMCT transitions.[24] This assignment is now supported by TD-DFT calculations on **11′**$^+$; the lowest-energy electronic transition principally involves the ligand-based β-HOMO−1 (2% Ru, 91% C≡CAr) to the Ru-based β-LUMO (64% Ru, 34% C≡CAr). In this work, *trans*-[Ru(16-TMC)(C≡CC_6H_4C≡CPh)$_2$]$^+$ (**12**$^+$) and *trans*-[Fe(dmpe)$_2$(C≡CPh)$_2$]$^+$ (**20**$^+$) show an intense absorption band at λ_{max} = 786 and 808 nm, respectively. It is significant to note that the $\pi(C{\equiv}CAr) \rightarrow d_\pi(Ru^{III})$ LMCT transition only slightly red-shifts in energy (by 1340 cm^{-1}) as the conjugation length *n* of [C≡C(C_6H_4C≡C)$_{n-1}$Ph] increases [λ_{max} = 14 060 and 12 720 cm^{-1} for **11**$^+$ (*n* = 1) and **12**$^+$ (*n* = 2), respectively]. This effect is relatively small as compared to the shift in MLCT transition (4570 cm^{-1}) for the corresponding Ru(II) species. A reasonable rationale for this is that the π(C≡CAr) level of *trans*-[Ru(16-TMC)(C≡CAr)$_2$]$^+$ is comparatively localized on the [C≡CC_6H_4] moiety rather than delocalized along the entire C≡CAr unit. This is supported by the similarity between the $E_{1/2}$ values of *trans*-[Ru(16-TMC)(C≡CAr)$_2$]$^{2+/+}$ for Ar = Ph (0.72 V) and C_6H_4C≡CPh (0.69 V), which are assigned as [C≡CAr]-centered oxidations. Recently, Humphrey and co-workers reported an intense NIR band for *trans*-[Ru(dppe)$_2$(C≡CPh)$_2$]$^+$ at 8920 cm^{-1} (1121 nm).[5g] Our TD-DFT calculations also support the occurrence of an absorption band for *trans*-[Ru(PH_3)$_4$(C≡CPh)$_2$]$^+$ at 1170 nm that is acetylide-to-ruthenium LMCT in nature. We suggest that such a LMCT transition exists for the dmpe-ligated species **1**$^+$−**3**$^+$ at similar energies, but we have not located the transition due to instrumental limitations of the spectroscopic window.

(E) Relationships between E_{MLCT}, E_{LMCT}, and $E_{\pi\pi^*}$. Intriguingly, we have found that the sum of the $d_\pi(M^{II}) \rightarrow \pi^*$-(C≡CAr) MLCT energy ($E_{MLCT}$) for *trans*-[$ML_4$(C≡CAr)$_2$] and the $\pi(C{\equiv}CAr) \rightarrow d_\pi(M^{III})$ LMCT energy (E_{LMCT}) for *trans*-[ML_4(C≡CAr)$_2$]$^+$ corresponds to the high-energy electronic absorption band for *trans*-[ML_4(C≡CAr)$_2$] ([ML_4] = [Ru(16-TMC)], [Ru(N_2O_2)], and [Fe(dmpe)$_2$]). For example, E_{MLCT} for **11** (25 190 cm^{-1}) + E_{LMCT} for **11**$^+$ (14 060 cm^{-1}) = 39 250 cm^{-1} (255 nm), and the high-energy absorption for **11** appears at 250 nm; E_{MLCT} for **12** (20 620 cm^{-1}) + E_{LMCT} for **12**$^+$ (12 720 cm^{-1}) = 33 340 cm^{-1} (300 nm), and the high-energy absorption for **12** is observed at 304 nm; E_{MLCT} for **20** (26 810 cm^{-1}) + E_{LMCT} for **20**$^+$ (12 380 cm^{-1}) = 39 190 cm^{-1} (255 nm), and the high-energy absorption for **20** occurs at 259 nm. TD-DFT

(33) Lewis, G. N.; Calvin, M. *Chem. Rev.* **1939**, *25*, 273−328.
(34) Recent examples: (a) Eisler, S.; Slepkov, A. D.; Elliott, E.; Luu, T.; McDonald, R.; Hegmann, F. A.; Tykwinski, R. R. *J. Am. Chem. Soc.* **2005**, *127*, 2666−2676. (b) Slepkov, A. D.; Hegmann, F. A.; Eisler, S.; Elliott, E.; Tykwinski, R. R. *J. Chem. Phys.* **2004**, *120*, 6807−6810. (c) Gibtner, T.; Hampel, F.; Gisselbrecht, J.-P.; Hirsch, A. *Chem.-Eur. J.* **2002**, *8*, 408−432. (d) Scemama, A.; Chaquin, P.; Gazeau, M.-C.; Bénilan, Y. *Chem. Phys. Lett.* **2002**, *361*, 520−524.

(35) The UV−vis spectra were recorded for a 1:1 mixture of *trans*-[ClRu(dmpe)$_2$-{C≡C(C_6H_4C≡C)$_{n-1}$$C_6H_4$$NO_2$-4}] and *trans*-[Ru(dmpe)$_2${C≡C(C_6H_4C≡C)$_{n-1}$$C_6H_4$$NO_2$-4}$_2$]. We have assumed that the lowest electronic transition energy for the bis-acetylide complexes is lower than that for their corresponding mono-acetylide derivatives.

calculations suggest that the high-energy transition for **11** and **12** is intraligand $\pi\pi^*$ in nature as anticipated. We suggest that the relationship $E_{MLCT} + E_{LMCT} = E_{\pi\pi^*}$ can be expected, provided that the energies of the π(C≡CAr), π^*(C≡CAr), and d_π(M) levels in both *trans*-[ML_4(C≡CAr)$_2$] and *trans*-[ML_4(C≡CAr)$_2$]$^+$ are similar. *Because this proposal is apparently true, the d_π(M) orbital can therefore be viewed as a localized "doped" level between the π(C≡CAr) and π^*(C≡CAr) levels.* Hence, when d_π(M) is fully occupied, only MLCT and $\pi\pi^*$ absorptions can be observed; when a vacancy is created in d_π(M) upon oxidation, the low-energy LMCT transition becomes accessible.

(F) Resonance Raman Studies. By simulating the MLCT absorption band and the resonance Raman intensities for **11**, it is apparent that the nominal $\nu_{C\equiv C}$ and $\nu_{C=C}$ stretch modes account for approximately 60% of the total vibrational reorganization energy, thus indicating that the absorption bands are strongly coupled to the C≡CPh ligand. Moreover, the reorganization of the C≡CPh ligand in the excited state is accompanied by reorganization of the Ru−C and Ru−N fragments (Franck−Condon active modes below 1200 cm^{-1}). This is consistent with the assignment that the absorption band is of MLCT character and reveals the existence of interaction between the Ru core and the C≡CPh moiety in the excited state.

General Remarks

Although π-back-bonding interaction for the Ru(II)−acetylide moiety has commonly been advocated, our experimental findings in this work suggest that the π-interaction is weak: (1) Ru−C distances for *trans*-[RuL_4(C≡CAr)$_2$] are similar for L_4 = (dmpe)$_2$ and 16-TMC; (2) Ru(III/II) redox potentials for *trans*-[RuL_4(C≡CAr)$_2$] are not sensitive to the conjugation effect of the acetylide ligands; (3) $\nu_{C\equiv C}$ values for coordinated acetylide ligands are similar for different chain lengths. Based on the notion that the interaction between $d_\pi(Ru^{II})$ and π/π^*(C≡CAr) is weak and the orbitals are localized, the $d_\pi(Ru^{II})$ can therefore be viewed as an isolated "doped" level that exists between the π(C≡CAr) and π^*(C≡CAr) levels. There are two major consequences of this: (1) a linear relationship is obtained between the MLCT (not intraligand) transition energy for *trans*-[Ru(dmpe)$_2${C≡C(C_6H_4C≡C)$_{n-1}$Ph}$_2$] and 1/*n*; and (2) the sum of the $d_\pi(M^{II}) \rightarrow \pi^*$(C≡CAr) MLCT energy for *trans*-[ML_4(C≡CAr)$_2$] and the π(C≡CAr) → $d_\pi(M^{III})$ LMCT energy for *trans*-[ML_4(C≡CAr)$_2$]$^+$ corresponds to the intraligand $\pi\pi^*$ absorption energy for *trans*-[ML_4(C≡CAr)$_2$].

It is pertinent to note the significant differences between the metal−carbon bonding interaction in ruthenium−acetylide and −cumulene complexes. In ruthenium−cumulene complexes,[15] the Ru−C π-interaction is strong and the π-system is delocalized throughout the [Ru=C=C=CAr$_2$] moiety. In contrast, for the ruthenium−acetylide complexes in this work, d_π(Ru) is only weakly coupled to the π-system of the [C≡CAr] moieties. We propose that the *trans*-[ML_m(C≡CAr)$_2$] class of complexes can be regarded as a model system for metal-doped carbon-rich π-conjugated wire materials, particularly for M = Ru. We have demonstrated that the $E_{1/2}$ values for the oxidation of *trans*-[RuL_4(C≡CAr)$_2$] can be varied by over 500 mV when L_4 changes from (dmpe)$_2$ to 16-TMC, λ_{max} of *trans*-[Ru(dmpe)$_2$-(C≡CAr)$_2$] can be adjusted by up to 6680 cm^{-1} when Ar changes from Ph to [(C_6H_4C≡C)$_2$Ph], and λ_{max} values for the oxidized M(III) species *trans*-[ML_4(C≡CAr)$_2$]$^+$ (M = Ru and Fe) are red-shifted by over 10 000 cm^{-1} as compared to *trans*-[ML_4(C≡CAr)$_2$]. These observations illustrate that the electrochemical and spectroscopic properties of *trans*-[RuL_4(C≡CAr)$_2$] can be systematically tuned by L_4 and Ar, because the energy of the $d_\pi(M^{II})$ level is controlled by the donor strength of the auxiliary ligand L_4, while the nature of Ar can define the energies of the π(C≡CAr) and π^*(C≡CAr) levels.

Acknowledgment. This work was supported by the Research Grants Council of the Hong Kong SAR, China, to C.-M.C. (HKU 7077/01P) and The University of Hong Kong. We thank the reviewers for helpful comments.

Supporting Information Available: CIF and crystallography data for **3**, **4**, and **5**, and perspective views of **4** and **5**; details of general procedures and instrumentations; supplementary characterization data and results sections; UV−visible spectra for selected complexes; tables of resonance Raman bands and simulation parameters for **11**; resonance Raman spectra and cross sections of **11**; tables of supplementary calculation results. This material is available free of charge via the Internet at http://pubs.acs.org.

JA053076+